Characterization of ALN thin films deposited by DC reactive magnetron sputtering

M. García-Méndez

Laboratorio de Nanociencias y Nanotecnología, Facultad de Ciencias Físico-Matemáticas de la UANL, División de Posgrado,
Manuel L. Barragán S/N, Edif. de Posgrado, Ciudad Universitaria, San Nicolás de los Garza, N.L. 66450, México,
e-mail: mgarcia@fcfm.uanl.mx

S. Morales-Rodríguez

Programa de Posgrado en Ingeniería Física Industrial, FCFM-UANL, División de Posgrado,
Manuel L. Barragán S/N, Edif. de Posgrado, Ciudad Universitaria, San Nicolás de los Garza, N.L. 66450, México.

R. Machorro and W. De La Cruz

Centro de Ciencias de la Materia Condensada de la Universidad Nacional Autónoma de México,
Km. 107, Carretera Tijuana-Ensenada, Ensenada, B.C. 22860, México

A set of AlN thin-films was prepared by reactive magnetron sputtering at room temperature. The purpose of this work was to study the effect of oxygen impurities on the structural and optical properties of *AlN* films. The structural and optical properties of the resulting films were characterized using X-ray diffraction (XRD) and spectroscopic ellipsometry, respectively. Depending on the deposition conditions, films can be hexagonal (wurtzite, P6₃m3) or cubic (zinc blende, Fm3m) in their microstructure. From the optical measurements, the ellipsometric parameters (ψ, Δ) and the real refractive index as a function of energy were obtained. From the ellipsometric measurements, a model of the Lorentz single-oscillator was employed to estimate the optical band gap, E_g.

Keywords: Reactive sputtering; thin films; AlN.

Se utilizó la técnica de erosión iónica reactiva para crecer películas delgadas de nitruro de aluminio (AlN). El propósito principal de este trabajo consistió en analizar el efecto del oxígeno en las propiedades ópticas y estructurales de las películas. Las propiedades estructurales y ópticas de las muestras se caracterizaron con espectroscopia elipsométrica y difracción de rayos X, respectivamente. La microestructura que pueden presentar las películas puede ser hexagonal (tipo wurzita, P6₃m3) ó cúbica (zinc-blenda, Fm3m), dependiendo de las condiciones de depósito. A partir de la medición de los parámetros elipsométricos (ψ, Δ), se utilizó el modelo del oscilador simple de Lorentz para obtener un estimado del ancho óptico, E_g.

Descriptores: Erosión iónica reactiva; películas delgadas; AlN.

PACS: 81.15.-Z, 68.55.-a, 82.80.-d

1. Introduction

Aluminum Nitride (AlN) is a material with a broad range of applications in electronic and optoelectronic devices due to its many physical and chemical properties. AlN has a high thermal conductivity (260 Wm^{-1}K^{-1}), a direct band gap (E$_g$=5.9-6.2 eV), high level of hardness (2×10^3 kgf mm^{-2}), high fusion temperature (2400°C) and a high acoustic velocity [1-6]. Polycrystalline AlN thin films oriented along the *c-axis* can be implemented as a part of integrated (Ultra Large Scale Integrated) devices, optical sensors in the *UV* range or in acoustic-optic devices [1-7]. The optimal performance of developing devices depends directly on the crystallographic and electronic properties of the AlN layer [3,4,8-10]. In addition, oxidized AlN (AlNO) is a material with good thermal and chemical stability. AlNO can be used as a protective coating and dielectric film in electronic circuits. With AlNO is possible to manufacture Metal Insulator Structures (MIS). For example, an AlNO film can replace the conventional passivating films of Si$_3$N$_4$ or SiO$_2$ on p-silicon solar cells [1-5]. AlNO has also been investigated as dosimetric

material for ionizing radiation and *UV* radiation. Besides, AlNO possesses a spectral sensitivity similar to that of human skin, which makes the AlNO a candidate material for use in medical applications for UV dosimetry [11].

AlN films (pure and oxidized) can be prepared using several techniques: chemical vapor deposition (*CVD*) [12-14], molecular beam epitaxy (MBE) [15,16], ion beam assisted deposition [17,18] or direct current (DC) reactive magnetron sputtering. Application of the magnetron technique facilitates the growth of polycrystalline AlN films on large substrates at a low temperature (as low as 200°C or even at room temperature) with the same properties as films obtained through CVD and MBE [19-22].

In a reactive-magnetron process, molecules of a reactive gas combine with the sputtered atoms from a metal target to form a compound thin film on a substrate. Thus, the optical, electronical and structural properties of the resulting films can be modified by the experimental deposition conditions. Due to the affinity of AlN for oxygen [23], AlN films may contain a surface oxide layer, which greatly influences the physical properties, and can modify the electronic structure

and promote shifts in luminescence peaks [24,25]. The luminescence properties of AlN are determined mainly by the presence of oxygen impurities in the host lattice [11]. In the design of optoelectronic devices, the correlation between the physical dimensions and the optical parameters requires that each optical parameter be determined as a function of wavelength as accurately as possible.

In this work, a set of samples were grown by reactive magnetron sputtering with varying deposition time, magnetron power, gas pressure and gas mixture. In this technique, it is well accepted that the properties of the films depend on deposition conditions such as substrate temperature, working pressure, gas flow rate and the incidence angle for sputtered particles. In general, the procedure for deposition consists in varying one deposition parameter at a time while keeping all others fixed, in an attempt to maximize a given thin-film property. The purpose of this work was to study the effect of oxygen impurities on the structural and optical properties of AlN films.

2. Experimental procedure

(a) Deposition of films

Depositions were carried out in a high-vacuum Pyrex chamber connected to a mechanic and turbomolecular pump (with a pumping speed of 100 lt/sec). Depositions started when the chamber reaches a base pressure of 1.33×10^{-6} mbar. The chamber was equipped with a magnetron on which the target was placed. The substrate holder was located 5 cm from the target. The substrate holder was equipped with a heater and a thermocouple. The magnetron was connected to a direct current (DC) energy power supply. The power supply made it possible to control the voltage (Volts) and to measure the current (Amperes) and power (Watts) on the target. The input of high purity gases (Ar, N_2, O_2: purity of 99.999 wt.%) into the chamber was controlled by individual rotometers. The gas pressure was measured using Pirani (from 1 bar to 6.6×10^{-3} mbar) and cold cathode (from 6.6×10^{-3} mbar to 1.33×10^{-6} mbar) gauges.

An aluminum disc (2.54 cm in diameter, 0.317 cm. thick, 99.99 % purity) was used as a target and glass slides were used as substrates. Substrates were rinsed in acetone used as the solvent, and ultrasonically cleaned before being placed in

the chamber. Inside the chamber, the aluminum target was sputter-cleaned with argon for 20 min. There was a shutter placed between magnetron/substrate during cleaning. After cleaning, the argon gas was replaced by a gas mixture previously prepared with a specific composition. Then the shutter was opened and deposition of the films in the gas mixture took place. For the growth of AlN films, the sputtering process was carried out with the mixture of $Ar+N_2$. For the growth of AlNO films, the sputtering process was carried out with the mixture of $Ar+N_2+O_2$. No heating was applied during the growth of the samples. The deposition process was carried out at a steady temperature of about 323 K. This temperature rose with the effect of heating because of the sputtering process on the target. The temperature was similar for each sample included here.

The experimental conditions utilized for the growth of thin films are summarized in Table I. For *Sample 1*, *Sample 2* and *Sample 4*, the sputtering process started with the gas mixture of $Ar+N_2$. For *Sample 3,* the sputtering process started with the gas mixture of $Ar+N_2+O_2$.

For *Sample 4*, the electronic properties at the surface level were characterized using X-ray Photoelectron Spectroscopy (XPS). Analyzing the surface reaction which takes place between Al with N_2 and O_2 can provide information about the nitride/oxide formation during the growth on the films at the substrate. The deposition conditions utilized in this sample can recreate to some extent the reaction mechanism that also takes place in the other samples.

(b) Characterization of films

Structural characterization of the films was performed by X-ray diffraction (XRD) methods using Philips X' Pert equipment (copper anode, K_α radiation, wavelength, λ=1.54 Å, step size 0.005°). Measurements were taken in theta/2theta scans of Bragg-Brentano geometry.

For indexation, the reflection peaks of the experimental diffractogram were compared with the standards of the JCPDS database [26]. Next, the PowderCell Software®was employed to determine the preferred orientation of the films. The fitting of lattice parameters was obtained using a multiple correlation analysis with a least squares optimization. The planes and angles were the variables. The lattice parameters "*a*" and "*c*" were the fitting constants.

TABLE I. Experimental conditions utilized for the growth of samples.

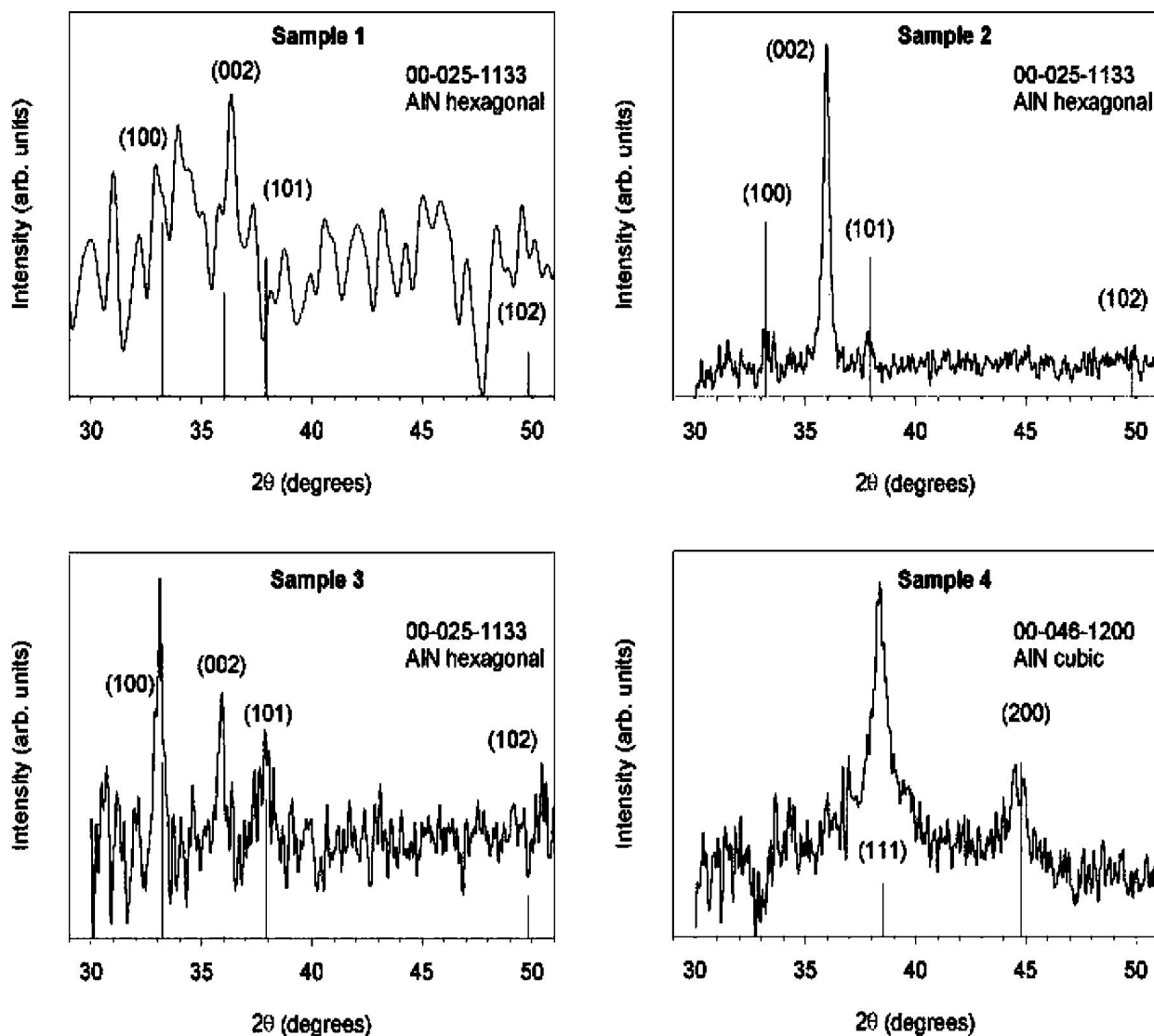| Sample	Deposition time (min.)	Voltage (Volts)	Power (Watts)	P_{Ar}	P_{Ar+N2}	$P_{Ar+N2+O2}$
					Pressure (x 10-3 mbar)	
1	10	300	150	9.3	12.5	*/
2	15	300	120	9.5	12.2	*
3	15	300	60	9.4	10.3	11.9
4	10	370	200	26.6	28.9	*

FIGURE 1. X-ray diffractograms for selected samples. Indexation taking the JCPDS files as standards is also included. The experimental conditions for deposition are presented in Table I.

The dielectric function, ε, film thickness, d, and the chemical composition of AlN films were determined by ellipsometry. When an incident linearly-polarized light impinged on the sample, the ellipsometer measured the amplitude (ψ) and phase (Δp change of the perpendicular component, "s", relative to the component "p" of monochromatic polarized-reflected light from a surface. The measurable parameters (ψ, Δp were related to the film and substrate using the complex reflectance ratio

$$\rho \equiv r_p/r_s = \tan \psi \exp(i\Delta), \qquad (1)$$

where "r_p" and "r_s" are the Fresnel reflection-coefficients for light polarized parallel and perpendicular to the plane of incidence, respectively.

Experimental ellipsometric measurements were obtained using a Woollam spectro-ellipsometer. Thickness and band gap of deposited samples are estimated by fitting a parameterized model to the measured data [27].

The electronic properties were characterized used an AES-XPS PHI 548 system (Al and Mg anode). An Ar ion gun mounted on the system was operated at 4 KeV by differential pumping. The equipment was calibrated using signals of pure Cu. For XPS, with the Mg anode, a pass energy of 100 eV was used to take the survey-spectra (scanning from 0-1200 eV), and a pass energy of 50 eV was used to take the high-resolution spectra (for the windows of Al2p, N1s, O1s and C1s signals).

From the XPS experimental measurements, the spectra obtained at the core level were curve-fitted using gaussian functions. Atomic concentrations were calculated from the peak areas of the Al2p, N1s, O1s transitions. Photoionization cross-sections for each element were taken into account to perform calculations of atomic concentration [28,29].

3. Results and discussion

The X-ray diffraction patterns of samples are shown in Fig. 1 (Intensity in linear scale *vs. 2θ*). In these diffractograms, the contribution of the substrate to the signal was subtracted.

The XRD pattern of *Sample 1* did not show well-defined crystalline features. For this sample, it appeared that the AlN layer was very thin. However, the diffractogram suggests the possible growth of a hexagonal structure.

For *Sample 2*, peaks at $2\theta = 33.1, 35.9, 37.8,$ and $49.8°$ were assigned to the $(100), (002), (101)$ and (102) reflections respectively, of a wurtzite hexagonal phase (group 186, file *00-025-1133*), with lattice parameters a=3.11 Å, c=4.97 Å [26]. The peak of highest intensity at $2\theta = 35.9°$ indicated that this sample is mainly formed by crystallites oriented along the [0001] *c-axis* direction.

For *Sample 3*, peaks at $2\theta = 33.1, 35.9,$ and $37.8°$ were assigned to the $(100), (002)$ and (101) reflections respectively. Similar to the *Sample 2*, reflections belonged to a wurtzite hexagonal phase (group 186, file *00-025-1133*) [26]. The peak of highest intensity at $2\theta = 33.1°$ indicated that this sample is mainly formed by crystallites oriented along the [-12-10] *a-axis* direction.

For *Sample 4*, peaks at $2\theta = 38.5$ and $44.7°$ were assigned to the (111) and (200) reflections respectively, of a zinc blende cubic phase (group 225, file 00-46-1200), with lattice parameter $a = 4.04$ Å [26]. The peak of highest intensity at $2\theta = 38.5°$ indicated that this sample is formed mainly by crystallites oriented in the [111] direction. For all samples, the varying deposition conditions produced films with different morphological features.

In this regard, it has been reported that the morphological properties of sputtered AlN films depend on the kinetics of arriving species and the surface migration of the atoms along the substrate [3,4]: at low pressure, sputtering species possess enough energy to form AlN layers of the hexagonal structure. Authors of Ref. 3 deposited AlN films by RF sput-

tering. They found a change in the orientation of the films from (002) to (001) directly related to the deposition pressure $(\sim10^{-3}$ mbar). In this case, the morphological differences were attributed to the changing pressure inside the chamber, which altered the direction, mobility and mean free path of the atoms. For our samples, the pressure used to grow the *Sample 2* and *Sample 3* was very similar (see Table I). However, for *Sample 3* there was a competition between the N_2 and the O_2 to react with *Al*. Also, it has been reported that oxygen can induce defects in the grow of AlN layers, producing a degree of amorphization [1,4,22,30]. For *Sample 4*, the chamber was more Ar-saturated than the other samples during the deposition process. This higher pressure in the chamber reduced the mean free path and the deposition rate of the sputtering species. Consequently, the kinetic energy was not high enough to form a wurtzite-like structure.

The ellipsometric measurements (ψ, Δp are presented in Fig. 2 for the three samples. The solid line represents the model response, while the broken line indicates the experimental measurement. The experimental and modeled curves were compared using a least squares process by minimizing

$$\chi^y g \sum [(\psi_m - \psi_e)^2 + (\Delta_m - \Delta_e)^2], \qquad (2)$$

where the subscripts "m" and "e" correspond to the modeled and experimental values, respectively. The equivalent refractive index of the composite layer was calculated using the effective-medium-approximation theory.

TABLE II. XPS calculation of relative elemental concentration (at.%) corresponding to *Sample A*. Characterization by XPS is included in Fig. 3.

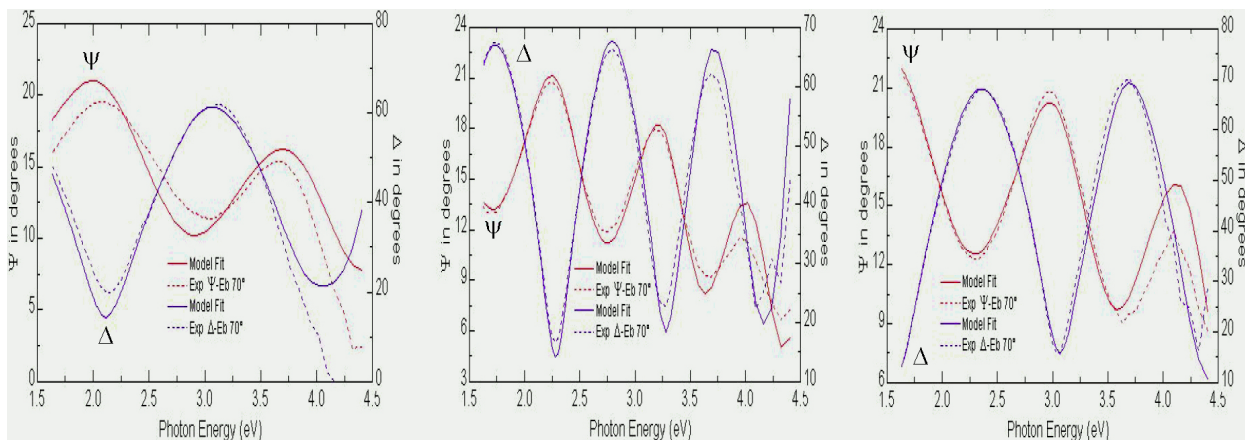| CONCENTRATION (at. %)					
Al + N +O			*Al + N*		
Al	*N*	*O*	*Al*	*N*	C(Al)/C(N)
47.0	11.9	41.0	79.7	20.2	3.9

FIGURE 2. Ellipsometric spectra for selected samples. Theoretical simulated-curves utilizing a three-layer model, Glass/AlN +voids/AlN+Al_2O_3+voids, are included. Parameters obtained from fitting are presented in Table II.
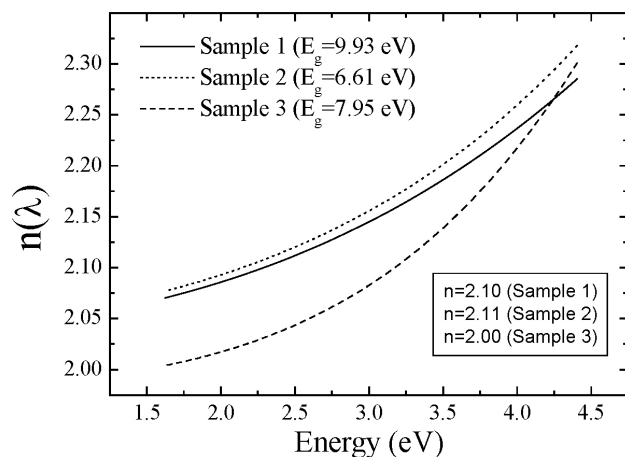
FIGURE 3. Variation of refractive index *vs.* photon energy (eV). At 2.3 eV, refractive index is $n = 2.10$ and $n = 2.11$ and $n = 2.0$ for *Sample 1, Sample 2* and *Sample 3*, respectively. .

The measurement of the parameters was repeated in order to ensure that fluctuations represented real signals and to discard noise. During film growth, there were differences in the obtained optical properties because of the changes in the preparation conditions.

As a first approach, the model compared the experimental optical data starting from a single homogeneous AlN layer.

Taking into account our deposition conditions (low pressure/temperature), the films were at the lower end of the Movchan-Demchishin zone model [31,32]. Apart from the columnar growth expected in films, experimental conditions produced voids in the AlN films [31]. Then, when voids were considered in the model, an improvement in the fitting was obtained. Considering the reactivity of the aluminum, a very thin layer of AlN at the top of the oxide layer is added. Thus, a mixture of layers, Al_2O_3+AlN+voids, was considered, producing a significant improvement in the fittings. Under our experimental conditions, the growth of the films is diffusion limited and hence void formation is likely.

The glass layer (SiO_2) was characterized and the optical data for Al_2O_3 were taken from Ref. 33. The volume fraction and thickness of the layers varied from sample to sample.

The refractive index model used in our simulation was expressed through the Lorentz dispersion equation:

$$\varepsilon(E) = \varepsilon_\infty + \frac{A}{(E_0^2 - E^2) - iBE}, \qquad (3)$$

where the parameter "A" is the oscillator amplitude, "B" is the broadening, "E_0" is the center energy location of the oscillator, that is, the resonance frequency of the material.

The method of the Lorentz oscillators describes the interaction between the electromagnetic field and an atom. However, this model is used widely to simulate the optical response of the material. The center energy location "E_0" is not formally related to the optical band-gap, E_g, but it provides a good idea of its position, if we argue that at "E_0" the material has its resonance frequency. At this frequency,

the material absorbs the light energy more efficiently. In the following lines, we shall consider this assumption to be valid.

The resulting parameters obtained from the ellipsometric measurements are included in Table II. The variation of the real refractive index (n) vs energy (eV) for the three selected samples is presented in Fig. 3.

Sample 1 and *Sample 2* were deposited with a similar gas mixture (see Table I). The difference between them was the deposition time, which accounted also for the differences in the estimated thickness (see Table II). For *Sample 3*, oxygen was added to the gas mixture during the sputtering process. The thickness of this sample was slightly lower than the value obtained for *Sample 2*, for a similar deposition time. For *Sample 3*, the difference in thickness could be explained on the basis of its lowest power (60 W, compared with 120 W for *Sample 2*). This loss of power could be attributed to a nitruration/oxidation of the target during the sputtering process. In the process, a layer of oxide/nitride was formed at the surface of the target. This layer acted as an electrostatic barrier for the impinging Ar^+ ions, which were able to promote a reduction in the deposition rate of the sputtered species.

Also from Table II, differences in the calculated values for the band gap can be observed. The band gap of E_g=9.9 eV of *Sample 1* did not fall within the values reported for AlN. In this case, it seems that the surface roughness and the oxide layer at the surface level contributed to a decreased intensity in the ellipsometric measurements. The band gap of this sample was similar to that reported for aluminum oxide. It has been reported that the composition of the AlO_x species, which could be the case for this sample, is very close to the stable Al_2O_3 [34].

For *Sample 2*, the calculated band gap of E_g=6.6 eV falls within the reported values for polycrystalline AlN thin films [35-37]. For *Sample 3*, the calculated band gap of E_g=7.95 eV was slightly higher than the value reported for AlN. In this case, the oxygen was introduced into the gas mixture during deposition. The oxygen content inside the resulting film could be the factor in the band-gap broadening.

From the graph of Fig. 3, the refractive indeces for *Sample 1*, *Sample 2* and *Sample 3* (at 533 nm, 2.3 eV) have a value of n=2.10, n=2.11 and n=2.02, respectively. The refractive index for AlN films has been reported in a wide range of values, including the following: n=1.9 for polycrystalline AlN films deposited by DC reactive sputtering [37], and n=2.1 for a bulk like AlN [37]; n=1.9 to 2.1 for polycrystalline AlN films deposited by DC reactive sputtering [19]; n=1.9 for highly textured [0001] oriented AlN films deposited by RF sputtering [35]; n=1.7 for [10-10] and [11-20] oriented polycrystalline AlN films deposited by DC reactive sputtering [35]. The authors of Ref. 37 report that an increase in the flow of N_2 during deposition tends to change the value of the refractive index. This change in value is attributed to a variation in the density of the films. The reported values of the refractive index for polycrystalline AlN films [19,35,37] cover our results obtained by ellipsometry. These results regarding the crystallinity are also supported by the XRD measurements.

Figure 4 displays the high-resolution XPS spectra of *Sample 4*, which were taken after 15 minutes of erosion with the *Ar* ion-gun. The deconvoluted curve for the Al2p, N2s and O1s transition-peaks are included. The peaks were composed of several contributions corresponding to Al, N, C and O in different chemical states. The Al2p transition was the sum of three individual components: Al-N (73.9 eV) [38,39], Al-O (75.6 eV) [38,40] and Al-C-O complex (78.1 eV) [41]. The $N1s$ transition contained the only component N-Al (397.8 eV) [38,41]. The $O1s$ transition was the sum of two components: O-Al (532 eV) [38,39] and $O-C$ (534.1 eV) [38,39]. This sample was not intentionally oxidized, but XPS detected traces of oxygen and carbon. In this case, O_2 remained in the chamber as a residual gas and C remained as an impurity. During the deposition process, this residual oxygen can react with the aluminum to form Al_xO_y compounds near the surface of the AlN film. The oxygen and carbon impurities can originate in the "dark zone" of the magnetron.

The results of the calculated atomic concentration are summarized in Table III. The column labeled Al+N$_2$+O$_2$" was the calculated elemental concentration taking into account the Al2p, N1s and O1s transitions. The column labeled "Al+N" was the calculated elemental-concentration taking into account the Al2p and N1s transitions. In this last case, the O1s transition was not considered in the calculation. The last column, C(Al)/C(N), was the ratio of aluminum to nitrogen concentration: this ratio was ≈3.9. With the area below

TABLE III. Contribution in percentage for the Al2p component corresponding to Sample A.

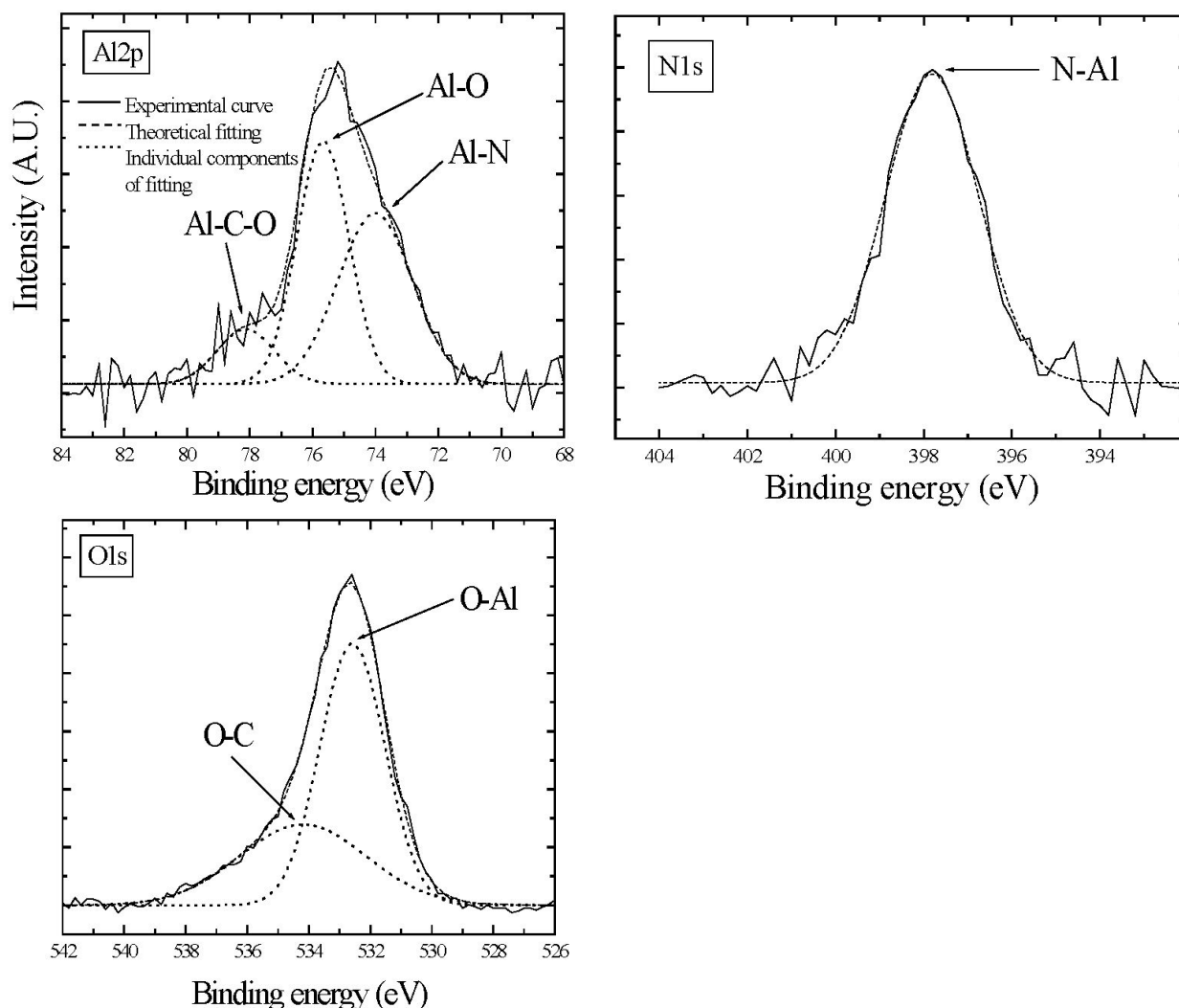| Al2p	
COMPONENT	*PERCENTAGE (%)*
Al-N	44.6
Al-O	44.2
Al-C-O	11.06

FIGURE 4. XPS spectra high-resolution windows for Al2p, N1s and O1s transitions corresponding to *Sample A*.

the curve of deconvoluted components "Al-N" (from "$Al2p$" transition) and "N-Al" (from "$N1s$" transition), the relative concentration obtained for Al and N was $\approx62.6\%$ and $\approx37.3\%$, respectively. Table IV presents the contribution in percentage (%) of each component for the Al2p transition. Taking into account the Al-N and Al-O components (not considering the Al-C-O component), it can be observed that the Al tends to react with N_2 and/or O_2 in almost the same proportion.

During the growth of AlN films, the AlO_x phase had been reported in great depth [22,38]. Based on microstructural observations, B.H. Hwang *et al.* of Ref. 22 proposed a growth mechanism for AlN thin films. In this model, the oxygen could react favorably with aluminum to form an amorphous Al_2O_3 layer, on which an AlN layer may start to grow. The oxide layer then induces stacking faults in the growing AlN layers. In thermodynamical terms, Al_2O_3 is more possible to form by gaseous phase reaction of $Al+(3/2)O_2$ than AlN of $Al+(1/2)N$, since $\Delta G(Al_2O_3)=-1480$ KJ/mol and $\Delta G(AlN)=-253$ KJ/mol [42].

From our results, the layers of AlO_x inducing stacking faults in the AlN layers seemed to be the case of *Sample 3*. On the other hand, the XPS results obtained from *Sample 4* seem to corroborate the similar tendency of the Al to attach to the N_2 and/or the O_2 during the growth of the film.

4. Conclusions

A set of AlN thin films was prepared by DC reactive magnetron sputtering. The following conclusions can be drawn:

Depending on the deposition conditions, AlN thin films can grow in a hexagonal or cubic microstructure. X-ray measurements indicated a polycrystalline mode of growth on films.

The refractive index measured for deposited samples corresponds to polycrystalline AlN thin films. The calculated band gap of 9.9 eV for *Sample 1* does not correspond to AlN. In this case, the surface roughness and the oxide layer at the surface level can contribute to a decreased intensity in the ellipsometric measurements, thereby affecting the band gap measurement. The band gap of 6.6 eV for *Sample 2* agrees with the reported values of AlN polycrystalline thin films. For *Sample 3*, a band gap of 7.9 eV is obtained. In this sample the oxygen also attaches to Al, forming an Al_xO_y layer. The layer can induce stacking faults throughout the film, tending to change the mode of crystal growth from polycrystalline to somewhat amorphous.

1. J. Chaudhuri *et al.*, *Mater Charac* **58** (2006) 672.

2. J. Olivares *et al.*, *Diam Relat Mater* **16** (2007) 1421.

3. J.P. Kar, G. Bose, and S. Tuli, *Vacuum* **81** (2006) 494.

4. K.H. Chiu, J.H. Chen, H.R. Chen, and R.S. Huang, *Thin Solid Films* **515** (2007) 4819.

5. K. Jang *et al.*, *Mat Sci Semicon Proc* **9** (2006) 1137.

6. G.M. Prinz *et al.*, *Superlattices Microst* **40** (2006) 513.

7. T.P. Drüsedau, T. Neubert, and A.N. Panckow, *Surf Coat Tech* **163-164** (2003) 164.

8. V.M. Pantojas, W. Otaño-Rivera, and J.N. Caraballo, *Thin Solid Films* **492** (2005) 118.

9. J.X. Zhang *et al.*, *Surf Coat Tech* **198** (2005) 68.

10. A.S. Gudovskikh *et al.*, *Sensors Actuators A-Phys* **113** (2004) 355.

11. L. Trinkler, B. Berzina, A. Auzina, M. Benabdesselan, and P. Iacconi, *Nucl Instrum A* **580** (2007) 354.

12. A. Sato, K. Azumada, T. Atsumori, and K. Hara, *J Crys Growth* **298** (2007) 379.

13. H. Uchida, M. Yamashita, S. Hanaki, and T. Fujimoto, *Vacuum* **80** (2006) 1356.

14. N. Takahashi, Y. Matsumoto, and T. Nakamura, *J Phys Chem Solids* **67** (2006) 665.

15. S. Iwata, Y. Nanjo, T. Okuno, S. Kurai, and T. Taguchi, *J Crys Growth* **301-302** (2007) 461.

16. P.D. Brown *et al.*, *J Crys Growth* **234** (2002) 384.

17. T. Matsumoto and M. Kiuchi, *Nucl Instrum B,* **242** (2006) 424.

18. K. Lal *et al.*, *Thin Solid Films* **434** (2003) 264.

19. Y.Z. You and D. Kim, *Thin Solid Films* **515** (2007) 2860.

20. J. R. Creighton, G.T. Wang, and M.E. Coltrin, *J Crystal Growth* **298** (2007) 2.

21. Q.X. Guo, T. Tanaka, M. Nishio, and H. Ogawa, *Vacuum* **80** (2006) 716.

22. B.H. Hwang, Ch.S. Chen, H.Y. Lu, and T.Ch. Hsu, *Mat Sci and Eng A* **325** (2002) 380.

23. V.A. Lavrenko, J. Desmaison, A.D. Panasyuk, and M. Deismaison-Brut, *J. Eur. Ceram. Soc.* **23** (2003) 357.

24. G.A. Slack, L.J. Schowalter, D. Moreli, and J.A. Freitas Jr., *J Crys Growth* **246** (2002) 287.

25. F. Ansart, H. Ganda, R. Saporte, and J.P. Traverse, *Thin Solid Films* **260** (1995) 38.

26. Powder Diffraction File, JCPDS International Centre for Diffraction Data, ICDD, Newtown Square, PA, 1998.

27. J.A. Woollam Co, *Ellipsometry Handbook and WVASE32^{TM} program* 2000.

28. J.C. Vickerman (editor), *Surface Analysis: the principal techniques*, 5a edición (John Wiley & Sons. 2005).

29. J.H. Scofield, *Journal Electron Spectros* **8** (1976) 129.

30. V. Brie and P. Pigeat, *J Cryst Growth* **299** (2007) 189.

31. R.F. Bunsha, *Deposition technologies for films and coatings* (Noyes Ed., Norwich, USA, 1982).

32. J.A. Thornton, *JVST* **11** (1974) 666.

33. S. Loughin, R.H. French, in (Ed.), *Handbook of Optical Constants of Solids III* (Academic Press, 1998, 373).

34. L.X. Benedict *et al.*, *Solid State Commun* **112** (1999) 129.

35. A.S. Gudovskikh *et al.*, *Sensor Actuat-A Phys* **113** (2004) 355.

36. J.M. Khoshman and M.E. Kordesch, *J non-Cryst Solids* **351** (2005) 3334.

37. S. Venkataraj, D. Severin, R. Drese, F. Koerfer, and M. Wutting, *Thin Solid Films* **502** (2006) 235.

38. A.M. Mahmood *et al.*, *Diamond and Related Materials* **12** (2003) 1315.

39. P.W. Wang, S. Sui, W. Wang, and W. Durrer, *Thin Solid Films* **295** (1997) 142.

40. J.F. Moulder, W.F. Sticke, P.E. Sobol, and K.D. Bomben, *Handbook of X-ray Photoelectron Spectroscopy*, 2a edición (Physical Electronics Division. Eden Prairie. 1992).

41. G.L. Fisher *et al.*, *Journal of the American Chemical Society* **124** (2002) 5528.

42. V. Brien and P. Pigeat *J Cryst Growth* **299** (2007) 189.